
Interaction between an eddy and a zonal jet Part II.

Two-and-a-half-layer model

Frédéric O. Vandermeirsch^{a,b,*}, Xavier J. Carton^{a,b} and Yves G. Morel^a

^a : Service Hydrographique et Océanographique de la Marine (SHOM), Centre Militaire d'Océanographie (CMO), Brest, France

^b : Institut Français pour l'Exploitation de la MER (IFREMER), Laboratoire de Physique des Océans (LPO), Brest, France

*: Corresponding author : Tel.: +33-2-98-22-4915; fax: +33-2-98-22-44-96

Abstract:

In a two-and-a-half-layer quasi-geostrophic model, a process study is conducted on the interaction between a vortex and a zonal jet, both with constant potential vorticity. The vortex is a stable anticyclone, initially located north of the eastward jet. The potential vorticity of the jet is allowed to have various vertical structures, while the vortex is concentrated in only one layer. The flow parameters are set to values characteristic of the Azores region.

First, the jet is stable. Weak vortices steadily drift north of the jet without crossing it while strong vortices can cross the jet and tear off a cyclone with which they pair as a heton (baroclinic dipole). This heton often breaks later in the shear exerted by the jet; the two vortices finally drift apart. When crossed by deep anticyclones, the jet develops meanders with 375 km wavelength. These results exhibit a noticeable similarity with the one-and-a-half-layer case studied in Part I.

Secondly, the jet is allowed to be linearly unstable. In the absence of the vortex, it develops meanders with 175 km wavelength and 25-day e-folding time on the β -plane. For various vertical structures of the jet, baroclinic instability is shown to barely affect jet-vortex interaction if the linear growth rate of unstable waves is smaller than $1/(14 \text{ days})$. Further simulations with a linearly unstable, nonlinearly equilibrated jet evidence its strong temporal variability when crossed by a deep vortex on the β -plane. In particular, long waves can dominate the spectrum for a few months after jet crossing by the vortex. Again in this process, the deep vortex couples with a surface cyclone and both drift southwestward.

Keywords: Rotating fluids; Stratified flow; Nonlinear equations; Jets; Vortices; Potential vorticity

1 Problem setting

In Part I of our study, we investigated the interaction between a stable jet and a stable vortex, both with constant potential vorticity, and confined in the upper layer of a stratified ocean. That study suggested that allowing a more complex vertical structure for the two features, and adding jet instability to this interaction could increase realism for an oceanic application. Therefore, we investigate here the interaction between a vortex and a zonal jet, for which baroclinic instability is allowed. The framework is a two-and-a-half layer quasi-geostrophic model, where both the vortex and the jet have constant potential vorticity. A possible application for the present study is the interaction between the Azores Current and meddies.

The Azores Current is the southern branch of recirculation of the Gulf-Stream in the northeastern Atlantic ocean. It flows quasi-zonally between $35^{\circ}W$ and $20^{\circ}W$ with maximum intensity (velocities reaching 0.3 m/s) above the thermocline (i.e. in the upper 800 meters). The variability of the Azores Current includes two essential components: a seasonal variation of its axis with latitude and the formation of mesoscale vortices due to baroclinic instability (Gould, 1985; Le Traon & De Mey, 1994; Kielmann & Käse, 1987). Occasionally, meanders of unusual length and amplitude form on the Azores Current; these meanders can occlude to form a cold cyclone south of the jet axis. In-situ measurements have shown that these features are associated with the passage of a meddy across and below the jet.

Meddies are intrathermocline lenses of Mediterranean water which detach from the Mediterranean undercurrents on the Iberian continental slope. These anticyclonic vortices can reach 100 km in diameter, 1000 m thickness and their center is located near 1000 m depth. They drift southwestward from their sites of formation, mostly under the influence of β -effect, of neighboring currents and of topography (Morel, 1995). In the course of this large-scale motion, they happen to cross the Azores Current as mentioned above. This crossing of the jet tears a surface-intensified cyclone which can temporarily couple with the meddy as a heton (a baroclinic dipole, see Tychensky & Carton, 1998; Richardson & Tychensky, 1998). Such an event was observed during the Semaphore 1993 experiment: figure 1 shows the horizontal maps of temperature at 200 and 1000 m and the observed meddy trajectory.

Numerical studies of jet-vortex interaction in one-and-a-half layer quasi-geostrophic models have shown that unstable jets could shed eddies when perturbed by a vortex (Bell & Pratt, 1992). On the contrary, when the jet is stable, the perturbation can be rapidly advected away from the eddy which generates it. Short-range jet-vortex interactions are very nonlinear and fragments torn off from the jet can pair with the vortex to form a dipole which propagates away.

In a two-layer quasi-geostrophic flow, Stern and Bidlot (1994) have determined the stationarity condition of a surface front in the presence of a vortex. They computed the meridional deviation of the front for a point vortex very far away from the front. In a one-and-a-half layer model, they calculated the mass and momentum flux associated with the entrainment inside the front. They observed that jet crossing by a vortex occurred for features of similar strengths.

This work was followed by a second study (Stern & Bidlot, 1995), again with a two-

layer quasi-geostrophic model, where the vorticity front and the vortex could have signatures in both layers. First, the authors considered the asymptotic limit of a very thick lower layer (compared with the upper one). They gave again an estimate for the area of fluid entrained into the shear flow, which was independent of the upper layer shear, even if this upper shear was much stronger than the lower one. With numerical experiments, they showed that the meridional drift velocity of the vortex was very dependent on its deep strength (area-integrated potential vorticity).

Yano and Flierl (1992) computed the deformation and the advection of a vortex in the presence of a shear or of a jet, in a two-layer quasi-geostrophic model on the beta-plane. Contour adjustment to the shear flow is dominant for small vortices with strong relative vorticity, while streamfunction adjustment by contour displacement occurs for large vortices with strong vortex stretching. The equilibrium vortex shapes, calculated analytically, evidence limits in vortex radius for stability. Nonlinearly, these limits correspond to the splitting of the vortex by the ambient shear.

The interaction of a vortex with an unstable, surface intensified coastal current was studied by Ikeda and Lygre (1989) with a two-layer quasi-geostrophic model. In the presence of a sloping bottom, cyclones are advected towards the coastal jet, travel upstream and can cross the jet; anticyclones induce meanders with wavelength of the fastest growing linear mode; they can couple with these meanders and generate new anticyclonic vortices.

The present paper addresses the following novel questions:

- what are the various regimes of nonlinear evolutions when the ratio of jet to vortex strengths and their vertical structures are varied ?
- can jet crossing by a vortex be analytically predicted ?
- what is the influence of jet baroclinic instability on jet-vortex interaction ?
- How does unstable jet forcing toward a zonal flow alter this interaction ?
- can specific features or characteristics be identified in jet vortex interaction which distinguish it from pure baroclinic instability ?

Section 2 presents the model equations and numerical implementation. Section 3 details the various evolutions of a vortex nearing a stable jet, when physical parameters are varied around those of the Azores region. In section 4, linear jet instability is allowed; the growth rates of normal-mode perturbations are computed. The interaction between a linearly unstable jet and a stable vortex is then studied, first in free-decay mode, then with weak relaxation of the jet towards a zonal state (section 5). Conclusions are drawn in section 6 regarding the questions listed hereabove.

2 Physical and numerical models

Mesoscale oceanic motions can be represented with a quasi-geostrophic model when planetary rotation and ocean stratification strongly constrain motions in the horizontal plane, and when the β -effect is moderate. The stratification of the ocean is idealized here as two-and-a-half layers (two active layers, here called upper and lower layers, over an infinitely deep layer at rest), with a rigid ocean surface.

2.1 The quasi-geostrophic equations

In the absence of forcing and of dissipation, the quasi-geostrophic equations express layerwise conservation of potential vorticity (hereafter PV);

$$[\partial_t + u_k \partial_x + v_k \partial_y] Q_k = 0 \quad (1)$$

where $k = 1, 2$ is the upper, lower (active) layer index and ψ_k is the streamfunction. Potential vorticity is

$$Q_k = \nabla^2 \psi_k - (-1)^k F_k (\psi_2 - \psi_1) - \delta_{2,k} F_3 \psi_2 + f_0 + \beta y$$

$F_k = f_0^2 L^2 / g_1' H_k$, ($k = 1, 2$), $F_3 = f_0^2 L^2 / g_2' H_2$ are the layer coupling coefficients. The reduced gravities are $g_1' = g(\rho_2 - \rho_1) / \rho_1$, $g_2' = g(\rho_3 - \rho_2) / \rho_1$. $\delta_{i,k}$ is the Kronecker symbol, and $H_1 / H_2 = 0.3$.

The flow can be decomposed to two baroclinic modes, with deformation radii defined by

$$\gamma_m^2 = 1 / R_{dm}^2 = 1/2 (F_1 + F_2 + F_3 \pm [(F_1 + F_2 + F_3)^2 - 4F_1 F_3]^{1/2}),$$

where $m = 1, 2$ are the two baroclinic mode indices; we set $\gamma_1 < \gamma_2$ (i.e. $R_{d1} > R_{d2}$). We call P the transfer matrix of layer to modes so that layerwise quantities are expressed in terms of modal quantities via $X_k = P_{km} X_m$.

2.2 Initial conditions

The initial conditions consist of a zonal jet with a circular vortex slightly distant from the jet axis (see figure 2). The jet is defined by two semi-infinite zonal strips of equal and opposite potential vorticity in each layer. The potential vorticity jump across the front at $y = 0$ is ΔQ_{Jk} in layer k . The jet velocity is, for each baroclinic mode m ,

$$v_{J,m}(y) = \frac{\Delta Q_{Jm}}{2\gamma_m} \exp(-\gamma_m |y|)$$

The vortex is a disk of radius R_T , with constant potential vorticity ΔQ_{Tk} in layer k ; it is initially centered at $y = y_T$. The azimuthal velocity created by this vortex is, for each baroclinic mode m ,

$$v_{T,m}(r) = \begin{cases} \Delta Q_{Tm} R_T K_1(\gamma_m R_T) I_1(\gamma_m r), & r < R_T \\ \Delta Q_{Tm} R_T I_1(\gamma_m R_T) K_1(\gamma_m r), & r > R_T \end{cases}$$

where r is the radial coordinate of the vortex; I_1 and K_1 are modified first-order Bessel functions of the first and the second kind, respectively.

In practice, only two cases must be studied: a cyclone or an anticyclone north of an eastward jet. All other cases (vortices south of the jet or westward jet) are deduced from the former two cases by symmetry of the quasi-geostrophic equations. Bearing in mind an application to meddies crossing the Azores Current, the case of an anticyclone will be studied in more detail. It can be anticipated physically that a cyclone north of an eastward jet should (most often) not cross the jet. With more complete physics (primitive equations), the case of a cyclone south of the jet should also be studied.

2.3 The numerical model

Jet-vortex interaction is studied here in a zonal channel. To model a potential vorticity front, a contour surgery algorithm would be best suited (see Dritschel & Saravanan, 1994). But such an algorithm is only available with periodic channel geometry. Unfortunately, periodicity creates spurious interference of waves which travel several times across the whole domain and thus perturb the local vortex-jet interaction. Only a finite-difference quasi-geostrophic model offers inflow-outflow boundary conditions (Holland, 1978). The drawback of the finite-difference code is the need to slightly smooth the vorticity fronts initially to avoid Gibbs' numerical instability. Nevertheless, a comparison performed between finite-difference and contour surgery models (when applicable) shows that this smoothing does not substantially alter the physics.

Therefore, the computational domain has inflow condition on the western side, radiative boundary condition on the eastern side and free-slip conditions along the northern and southern walls. All model parameters have been rendered dimensionless by setting the vortex radius to unity, $R_T = 1$, and the maximum potential vorticity jump across the jet (over the two layers), $\Delta Q_{Jk} = 1$, $k = 1$ or 2 . In dimensionless terms, the computational domain length is $L_x = 18.75$. Since the horizontal resolution is 151×151 nodes, the grid mesh is $\Delta x = \Delta y = 0.125$, and the time-step is computed from the Courant-Friedrich-Levy stability condition.

For an application to the Azores Current and to meddies, a typical value of vortex radius $R_T^* = 40$ km and maximum jet velocity $U^* = 0.24$ m/s³ were used to transcribe model results into oceanic values.

The numerical model is only weakly dissipative: biharmonic viscosity removes enstrophy accumulation at small scales. This does not alter the physical evolution of the flow compared with the inviscid case. In section 4, a slow relaxation of the flow toward the mean zonal jet $\bar{\psi}_k$ will also be used. Equation (1) is therefore written in the most general case

$$[\partial_t + u_k \partial_x + v_k \partial_y] Q_k = -\nu \nabla^6 \psi_k - r_k (\nabla^2 \psi_k - \nabla^2 \bar{\psi}_k) \quad (2)$$

3 Interaction between a vortex and a stable jet; sensitivity to relative intensities

Here, the generic behaviors of the jet-vortex system are determined when varying the physical parameters (jet and vortex potential vorticities, deformation radii) around values characteristic of the Azores region (see table 1). In all of this section, the jet is stable and β -effect is neglected.

With a jet confined in the upper layer ($\Delta Q_{J1} = 1, \Delta Q_{J2} = 0$) and a vortex lying in the lower layer ($\Delta Q_{T1} = 0, \Delta Q_{T2} = \Delta Q_T$), three nonlinear regimes are observed when increasing ΔQ_T (see figure 2a of part 1):

1) for $|\Delta Q_T| < \Delta Q_{Tc}$ (here $\Delta Q_{Tc} = 1.8$), the vortex drifts along the jet without crossing it;

³the maximum jet velocity in the model is 0.16

- 2) for $\Delta Q_{Tc} < |\Delta Q_T| < \Delta Q_{Tc} + \delta q$ (here $\delta q = 0.35$), the vortex crosses the jet and tears a cyclone away from it; the two vortices form a heton whose direction of propagation depends on their relative strengths (see figure 2b of part 1);
- 3) for $|\Delta Q_T| > \Delta Q_{Tc} + \delta q$, the vortex crosses the jet without heton formation, and finally drifts eastward south of the jet.

These three regimes are very general (only the numerical values of ΔQ_{Tc} and of δq vary with the physical parameters). Indeed, these regimes have been obtained with all stable distributions of jet and vortex potential vorticity (non zero potential vorticity in each layer separately or in both layers simultaneously).

Varying the jet and vortex potential vorticities or the deformation radii within realistic values for oceanic applications (see table 1) does not qualitatively alter this outcome: the jet is allowed to have various ratios of upper to lower layer PV, while the vortex is confined in any single layer. The trapping of weak vortices north of the jet is replaced by jet crossing when the vortex is stronger than a critical value which depends on the jet PV. The intermediate regime with heton formation is most often observed.

Two of these regimes are now described in more details:

- In regime 1 (experiment 1a), the vortex becomes elliptical in the shear of the jet; this vortex also induces a long meander on this jet; after a short adjustment period, they both propagate zonally (see figure 3a). The scatter plot of potential vorticity versus relative streamfunction (in the moving frame of reference) does not show a specific correlation during the adjustment period, but in the long term, it is quasi linear with very little dispersion (see figure 3b); a steady state is then attained.
- In regime 2 (experiment 1b), the anticyclone rapidly crosses the jet, shedding few filaments (see figure 3c); the southward meander of this jet undergoes occlusion to form a cyclone. The heton thus formed propagates westward (upstream of the jet), in a similar manner to meddy Encelade south of the Azores Current, during the Semaphore experiment (Tychensky & Carton, 1998). Since the anticyclone is stronger than the cyclone, this trajectory curves back progressively towards the jet, whose shear exerted on the heton increases with time. Eventually, the heton is torn apart, and the separate vortices drift eastward along the jet.

To obtain an analytical criterion for jet crossing by the vortex, we observe that the interaction between the jet and the vortex is achieved by vortex stretching between the upper and lower layers, and is carried out mostly by the density interface between these layers. This interface displacement is best represented by the first baroclinic mode. Therefore, we transpose to this baroclinic mode the layerwise criterion on velocities used in part I: *the vortex will cross the jet if the projection of its velocity on the first baroclinic mode is equal and opposite to that of the jet on the same mode*. If the vortex lies in layer k , and whatever the vertical structure of the jet, this criterion is written mathematically:

$$\frac{|\Delta Q_{J1}|}{|\Delta Q_{Tk}|} = \frac{2R_Q P_{12}}{R_Q P_{22} - P_{12}} \gamma_1 R_T I_1(\gamma_1 R_T) K_1(\gamma_1 R_T)$$

with $l = 3 - k$, $P_{22}/P_{12} = F_2/(F_2 + F_3 - \gamma_2^2)$, $R_Q = \Delta Q_{J1}/\Delta Q_{J2} > 0$. ΔQ_{Tk} is the

critical vortex intensity for jet crossing.

This criterion assumes that the first baroclinic mode captures the vertical distribution of motions adequately; this is the case for many oceanic motions. This also explains why this criterion works well with our flow parameters, chosen to fit the Azores region. The predictions of the criterion lie within 25% of the values found numerically here. Since many stable vertical distributions of potential vorticity have been considered here (see table 1), we can conclude that this criterion works in fairly general cases.

Moreover, our results are consistent with the Stern and Bidlot (1995) study: indeed, in the asymptotic limit $H_1/H_2 \ll 1$, the baroclinic flow reduces to the lower layer velocity. Our criterion is then written $V_{\theta,2} = -U_{J,2}$, where $V_{\theta,2} \propto \Gamma_2 L$ (Γ_2 the integrated PV of the vortex and L a horizontal length scale) and $U_{J,2} \propto s_2 L$ (s_2 the shear of the jet). Therefore, fluid entrainment into the jet region will depend only on s_2 .

This can be understood also from the point of view of the dynamical equations: the quasi-geostrophic equations are the shallow-water equations integrated over the layer thickness. Any potential vorticity anomaly will be influential proportionally to its *volume* integral in the shallow-water equations. In the quasi-geostrophic equations, this reduces to area integral since layer thicknesses are nearly constant. This explains why, in the limit $H_1/H_2 \ll 1$, the influence of the upper layer shear s_1 is negligible compared with that of s_2 even if $s_1 > s_2$.

Three complementary observations can be made here:

a) the value $\Delta Q_{T_c} \sim 2$ obtained numerically as characterising the boundary between regimes, is important: indeed, with our choice of parameters, it lies in the range given by our analytical criterion for jet crossing;

b) these numerical results and analytical criterion have been obtained on the f -plane; adding β -effect does not strongly modify the conditions for jet crossing by the vortex. Nevertheless, it will noticeably alter the final trajectory of the anticyclone, which will be mostly southwestward instead of along the jet axis.

c) an application to the Azores jet and meddies, as observed during the SEMAPHORE experiment, with a qualitative estimate of jet PV, leads to a vortex to jet Ertel PV ratio between 2 and 3 (see plate 3 of Tychensky et al., 1998, and plate 12 of Tychensky and Carton, 1998). The crossing criterion derived here is therefore consistent with the observed crossing of the Azores Current by meddy Encelade.

4 Influence of jet instability

All previous work of Part 1 and Part 2 was performed with stable jets. In the ocean, jets are often linearly stable and undergo meandering. Therefore we have to consider the interaction between a vortex and a meandering jet. Hereafter, jet instability is allowed by setting negative values for its potential vorticity jump in the lower layer (its upper layer potential vorticity jump is +1). Indeed, the sign reversal between ΔQ_{J1} and ΔQ_{J2} satisfies the Charney-Stern criterion. The vortex has potential vorticity in the lower layer only.

4.1 Linear instability of the jet in the absence of the vortex

First, linear jet stability is investigated in the absence of the vortex to determine the time scales associated with meander growth via baroclinic instability.

The linear instability equation is derived from equation (2) where the very weak biharmonic dissipation is neglected. Linear relaxation of the flow towards a zonal state will be used in subsection 5.2 and its effect is included in the linear instability equation.

The flow is decomposed in mean zonal jet (overlined variables) and perturbation (primed variables): $\psi_k = \bar{\psi}_k + \psi'_k$ so that

$$\partial_t Q'_k + J(\bar{\psi}_k, Q'_k) + J(\psi'_k, \bar{Q}_k) = -r_k \nabla^2 \psi'_k$$

The perturbation is a normal mode:

$$\psi'_k(x, y, t) = \text{Re}[\phi_k(y) e^{ik(x-ct)}]$$

where $\text{Re}(c)$ is the phase speed and $k\text{Im}(c)$ is the growth rate of perturbations. Note that ϕ_k is even in y (sinusoidal meander).

With these definitions, the linear instability equation is

$$(\bar{u}_k - c - i\frac{r_k}{k}) Q'_k + \psi'_k \frac{d\bar{Q}_k}{dy} = 0.$$

The perturbation can be calculated as

$$\phi_m = A_m \exp(k_{\gamma m} y) + B_m \exp(-k_{\gamma m} y)$$

for the vertical mode m with $k_{\gamma m}^2 = k^2 + \gamma_m^2$. Continuity of pressure and integration of the linear equation across the vorticity front lead to a quadratic dispersion relation in c . Note that when the layers are decoupled, the usual 1-1/2 layer dispersion relation is recovered.

The potential vorticity jump across the jet in the lower layer is set to $\Delta Q_{J2} = -0.1$ to generate velocity profiles close to those of the Azores Current. Baroclinic instability is then obtained; Figure 4a shows the growth rates and phase speeds in the unforced case ($r_1 = r_2 = 0$). As usual for baroclinic instability, a long wave cut-off is observed. Maximum instability is found for $k \approx 1.43$ ($\lambda \approx 175$ km); the time-scale for exponential growth of the perturbations (hereafter called e-folding time) is $T_c \approx 20$ days on the f -plane; this value is close to oceanic observations.

When relaxation is added, growth rates decrease linearly with r_k (not shown); this result is identical to that of the Phillips model with linear friction (Pedlosky, 1987). In subsection 4.2, the value $r_k = 0.001$ is used for jet relaxation towards a zonal state. This corresponds to a relaxation period $T_r = 430$ days, for which the growth rates are identical to those at $r_k = 0$. When reducing the relaxation period to $T_r = 43$ days ($r_1 = r_2 = 0.01$), the maximum growth rate becomes only half as large as that at $r_k = 0$, and the range of unstable wavenumbers shrinks noticeably (see figure 4b); nevertheless, the most unstable wavenumber is identical ($k \approx 1.43$).

A similar decrease of maximum growth rates and of the range of unstable wavenumbers is observed when β -effect is introduced; wavenumber $k \approx 1.43$ ($\lambda \approx 175$ km) remains the most unstable (figure not shown); for a value of β corresponding to the latitude of the Azores Current, the e-folding time of the most unstable perturbations is $T_c \approx 25$ days.

4.2 Initial-value problem of vortex-unstable jet interaction

In this section, we study the initial value problem of vortex interaction with a linearly unstable jet, for which no relaxation towards the mean flow is imposed. The deep potential vorticity of the jet is varied to obtain different growth rates for baroclinic instability and to test the sensitivity of the interaction to this factor. The values of the other parameters are given in table 2. The computational domain length is $L_x = 18.75$, so that wavenumbers k obtained in the linear study (subsection 4.1) must be renormalized here as mode $n = (L_x/2\pi)k$. Experiments are performed successively on the f -plane and on the β -plane.

As a general rule, three nonlinear regimes are observed, which depend on the e-folding time T_c of jet instability:

- for $5 < T_c < 10$ days, the jet evolution is very unstable and jet crossing by the vortex is unpredictable; the vortex trajectory is erratic;
- for $10 < T_c < 14$ days, the vortex always crosses the jet, but unrealistically large jet meanders perturb its trajectory for a long duration;
- for $T_c > 14$ days, the vortex crosses the jet, while meanders have wavelengths and amplitudes comparable with those observed in the Azores region.

Figure 5a (resp. 5b) presents the jet and vortex evolution on the f -plane (resp. on the β -plane), when the e-folding time scale of unstable waves is $T_c = 13$ days (resp. 20 days); these simulations are respectively experiments 2a and 2b. Large-amplitude meanders, with meridional extent equal to 300 km, form on the jet, with mode $n = 2$ (375 km). These waves are twice as long as those resulting from the baroclinic instability of the jet. After some time, they occlude to generate one or two cyclones south of the jet. These cyclones merge with the jet after a few months. On the f -plane, the anticyclone moves southeastward as in the stable jet case, but more slowly. On the β -plane, it drifts southwestward quite rapidly; in particular it crosses the jet with a meridional velocity close to 2 cm/s.

Results for a less unstable jet ($T_c = 25$ days) are closer to oceanic observations: jet meanders only reach 200 km in meridional amplitude, the anticyclone crosses the jet axis with $v \approx 4$ cm/s and the heton formed with the cyclone moves upstream of the jet (figure not shown). This evolution of the anticyclone is very similar to that in the stable jet case.

5 Interaction of a vortex with a forced unstable jet

For more realism regarding oceanic observations, we now consider a linearly unstable jet which stabilizes in a non-zonal configuration before the vortex is introduced in the flow field. Indeed meddies interact with the Azores Current while it is in a non-zonal state.

5.1 Jet forcing and equilibration

Here, the zonal jet is initially perturbed with a sinusoidal wave:

$$\psi'_k(x, y, t = 0) = \psi_0 \sin(kx) / \cosh^2(y/R_{d1})$$

where $|\psi_0| = |\bar{\psi}|/1000$ and $k = 1.43$ ($n \approx 4$) is the linearly most unstable wavenumber. Its e-folding time is $T_c = 20$ days.

Equilibration is attained by weakly relaxing potential vorticity towards the initial zonal jet (see equation (2)). Physically, this nudging term allows a relaxation towards a sharp PV front and does not alter baroclinic instability considerably, while large-scale heat or mechanical (wind-stress) forcing would smooth out the front and inject energy into the baroclinic mode, thus altering the characteristics of linear baroclinic instability. We also note that such a relaxation procedure has already been used for similar purposes in other studies (Pedlosky, 1992; Rivière, 1995). Finally, since the relaxation coefficient is weak ($r_k = 10^{-3}$), the relaxation period is much longer than the average duration of jet crossing by the vortex (430 days compared with 20 days). The balance between relaxation and linear instability also allows a limited number of eddy shedding during the equilibration period.

Biharmonic viscosity is $\nu = 3 \cdot 10^{-6}$ in the early stage of the simulation. But a weaker dissipation ($\nu = 4 \cdot 10^{-7}$) is used during the long stage of nonlinear equilibration to avoid excessive enstrophy dissipation. With these values, the ratio between forcing and dissipation ($r_k(\delta x)^4/\nu \in [0.1, 0.6]$) leads to an energy balance in the long term: the numerical model has been integrated for 7 years to reach a finite-amplitude equilibrium of the jet. The final jet is - statistically (in the time-averaged sense) - in equilibrium with its meanders and shed eddies.

The equilibrated states of the jet exhibit meanders with periodic, aperiodic and quasi-stationary evolutions depending on r_k and β (see table 3; see also Rivière, 1995):

- experiment 3a is performed on the f -plane in free-decay (no relaxation of the jet). First, the linearly most unstable wave ($n = 4$) grows until a vortex is shed; the unstable jet then equilibrates in an aperiodic regime and long waves (successively $n = 3, 2, 1$) dominate in the jet perturbation (see figure 7a; consider the portion of the plot left of the vertical dashed line, i.e. before the vortex is added). Indeed, in the absence of β -effect and of forcing, nonlinear effects restabilize short waves preferentially (Rivière, 1995). This evolution also agrees with quasi-geostrophic simulations of Gulf-Stream instability (Flierl et al., 1999) and with the energy cascade toward large scales in two-dimensional turbulence. Note that more unstable jets (e.g. with $T_c = 11$ days) do not equilibrate nonlinearly, lose their zonal coherence and fragment.
- experiment 3b is performed again on the f -plane, but with relaxation of the jet

towards the zonal flow. The jet equilibrates nonlinearly in an aperiodic regime where mode $n = 2$ dominates (see figure 7b, left of the vertical dashed line).

- experiment 3c is performed on the β -plane without relaxation of the jet. Comparing the nonlinear jet equilibria with the f -plane experiment (3a) shows that β -effect halts the energy cascade towards large scales. In particular, the dominant wave at finite-amplitude stabilization is now $n = 2$ (see figure 9a, left of the vertical dashed line).

- experiment 3d is again performed on the β -plane, but now with relaxation of the jet. The baroclinic instability of the jet first forms mode $n = 4$; then mode $n = 3$ equilibrates nonlinearly in an aperiodic regime (see figure 9b, left of the vertical dashed line).

- finally, experiments 3e is performed with jet relaxation and a stronger β effect. Mode $n = 4$ grows the fastest linearly and it is followed in time by wave $n = 3$ which eventually dominates slightly (see figure 10).

5.2 Jet-vortex interaction

The vortex is then introduced in the numerical model and its interaction with the non-zonal jet is studied both on the f -plane and on the β -plane (see tables 3 and 4).

5.2.1 f -plane experiments

In experiment 3a, the anticyclonic vortex introduced north of the jet crosses it. The anticyclone tears off a cyclonic vortex south of the jet (see figure 6a). The large meander accompanying this process then interacts with a pre-existing cyclone created during jet equilibration. No specific signature of jet crossing by the anticyclone is noticed in the time evolution of the wave spectrum (see figure 7a). Introducing a cyclone south of the equilibrated jet also leads to jet crossing and to a similar evolution of the wave spectrum with time.

In experiment 3b, the anticyclone introduced north of the jet crosses it, tearing off a cyclone (see figure 6b). No specific signature is noticed in the wave spectrum at this instant (see figure 7b), but for a small peak on $n = 3$ (this short wave signals the localized interaction). The following small peak on $n = 1$ at model time $t = 5000$ corresponds to the merger of the cyclonic vortex with the jet.

In conclusion, the interaction of both unforced and forced jet with a vortex on the f -plane, does not exhibit a clear signature in the wave spectrum. Moreover, though vortices are produced by the interaction, they are rapidly reabsorbed by the jet and they cannot be easily distinguished from vortices resulting from baroclinic jet instability.

5.2.2 β -plane experiments

In experiment 3c, the anticyclone crosses the jet and couples with a cyclone; this heton propagates southwestward (figure 8a). This crossing is accompanied by a noticeable growth of all waves; but mode $n = 2$ remains the dominant one by large (figure 9a). Then, all waves undergo a slow decrease except $n = 1$ which oscillates. The presence of this long wave can result initially from the detachment of the cyclone

(Flierl et al., 1999), and later from the interaction of the jet with the distant heton.

In experiment 3d, the forcing is introduced and it physically results in a more localized perturbation when the vortex crosses the jet (figure 8b). Again the anticyclone couples with the cyclone and they propagate southwestward. The crossing of the jet is well characterized in the wave spectrum: modes $n = 1, 2$ grow significantly while modes $n = 3, 4$ weaken (figure 9b). Modes $n = 2$ (375 km wavelength) is again the strongest for 5 months following the jet-vortex interaction; afterwards, modes $n = 3, 4$ become dominant again.

Finally, in experiment 3e, the introduction of the anticyclone and its interaction with the jet again lead to the rapid growth of mode $n = 2$; modes $n = 1, 3$ grow and mode $n = 4$ decreases (figure 10). Finally, short waves dominate again with a fast oscillation as before vortex introduction.

In conclusion, when the jet is not relaxed, adding β -effect results in a clear jump in wave amplitudes. But these amplitudes then vary little, so that in the ocean, such a jump could not be easily attributed to vortex crossing rather than to a variation in external forcing for instance. On the contrary, the combination of β -effect and jet forcing allows the characterization of jet crossing by the vortex by a large-amplitude, finite-time signal in the wave spectrum. Mode $n = 2$ emerges from the short waves which result from nonlinear equilibration, and decays after a few months. In physical space, hetons are produced by the jet-vortex interaction and they clearly drift southwestward, maintaining their identity for a significant duration.

5.2.3 Influence of β -effect and of the ratio of vortex to deformation radii in the forced jet experiments

As seen hereabove, for forced jet experiments, the dominant wavenumber changes when the vortex is introduced in the flow, both on the f -plane and on the β -plane. This change in wavenumber is only weakly dependent on β effect and on the ratio of vortex to deformation radii (see figure 11-a and b). For all realistic ratios of vortex to deformation radii considered here, mode $n = 2$ is dominant in the jet perturbation, during jet-vortex interaction on the β -plane. The second largest wave has a long wavelength when the jet interacts with large vortices.

Finally, it must be noted that varying the ratio of vortex to jet PV (in the range [1.8; 2.5]) does not induce substantial changes in the physical results described hereabove.

6 Summary and conclusions

The interaction between a stable vortex and a stable or unstable jet, has been explored in a two-and-a-half layer quasi-geostrophic model. The vortex was confined in a single layer (most often the lower one), and the jet had various vertical structures (the choice of a surface-confined jet was finally made for an application to the Azores Current).

For stable, weakly unstable or nonlinearly stabilized jets, three nonlinear regimes have been observed:

- 1) absence of jet crossing by weak vortices which drift zonally north of the jet,
- 2) jet crossing by vortices with medium strengths, leading to dipole formation and splitting, and
- 3) jet crossing by strong vortices without dipole formation.

On the f -plane, anticyclones drift along a stable jet after crossing it; this drift is most often downstream and quasi-steady. Large anticyclones can fragment when crossing the jet (cf Käse & Zenk, 1996). Adding β -effect will favor southwestward trajectories of anticyclones after jet crossing.

For stable jets, the crossing criterion of Part I was generalized to the first baroclinic mode; though empirical, this criterion agrees fairly well with numerical experiments, for various vertical structures of the vortex and jet.

Linear jet instability was then considered: its growth rates were computed with and without relaxation or β -effect. In the absence of relaxation and of β -effect, meanders with 175 km wavelengths grow the fastest (20-day e-folding time on the f -plane, increasing to 25 days with β -effect). Substantial relaxation is needed to increase this e-folding time. These instability characteristics are realistic in the Azores region.

Then, initial-value simulations of vortex interaction with a linearly unstable jet in free-decay showed that nonlinear growth of perturbations on the jet can strongly perturb jet-vortex interaction if their e-folding time is smaller than 14 days. For weaker instability, the characteristics of jet-vortex interaction are comparable to those of the stable jet case. Then, the crossing criterion still applies, and meander wavelengths during crossing are close to 375 km, much larger than those of baroclinic jet instability.

Finally the interaction of a vortex with a non zonal jet was studied. The unstable jet was brought into equilibrium with its meanders and eddies via a slow relaxation towards a zonal flow, before the vortex was introduced north of its axis.

On the f -plane, the interaction between the vortex and the equilibrated jet cannot be unambiguously detected by the dominant wavelength in the spectrum. In physical space, it is equally difficult to identify the formation of a heton south of the jet, because of the mesoscale activity due to baroclinic instability. Furthermore, the life-time of this heton is often short, if it even exists.

On the β -plane, a characteristic meander wavelength (375 km) clearly dominates the other waves on the nonlinearly equilibrated jet when it is crossed by the vortex. This wavelength, quite different from that of baroclinic jet instability (175 km), dominates the spectrum whatever the vortex radius, strength and the β -effect (within realistic values). Moreover, the dominance of this wave lasts for a few months, thus providing a distinct signal of jet-vortex interaction in the wave spectrum. In physical space, jet-vortex interaction can also be identified by the formation of a heton which propagates rapidly. Finally, the radius of the incoming vortex is characterized by the second dominant wave in the spectrum.

These results are original with regard to previous studies and may help meddy detection from indirect signature at the surface. This could be performed with the help of sea surface height and temperature maps at short time intervals (10 days or less). During that duration, meanders propagate less than 1/4 of the wavelength of baroclinically unstable waves and 1/9 of the wavelength of meanders due to jet-vortex

interaction. Coherent feature analysers, already available in forecast centers, could help identify the frontal zones, compute the dominant wavelengths of meanders and displacement of eddies. Such an automatic procedure could help detect Azores Current crossing by a meddy if a northward meander is first formed (vertical alignment of negative vorticity with the underlying meddy), followed by a southward meander which occludes as a cold cyclone, leading to long waves on the jet and to complex vortex motion south of the jet. It should also be investigated if a direct SST or SSH signature of the meddy is then visible south of the jet. This whole process is well described by figure 2 of Richardson and Tychensky (1998) and clearly corresponds to our numerical simulations in the forced case on the β -plane.

But we must keep in mind that our framework is idealized:

- the vertical structure retained in our model is very simple. More complex vertical structures would on the one hand have direct impact on mesoscale dynamics : they would a priori increase the energy in the low baroclinic modes via the catalytic effects of the high modes (Barnier et al., 1991) and thus reinforce the validity of our analytical criterion. On the other hand, reaching finer vertical and horizontal scales could imply taking into account submesoscale dynamics (in particular via primitive equation modeling). Recent studies of submesoscale effects in jet instability (Levy et al., 2001) reveal that they mostly favor filament formation and robustness. In our study, filaments are mostly present once the vortex has crossed the jet.

- no surface turbulence or waves are taken into account while they tend to hide meddy signature at the ocean surface. Presently, meddy detection and tracking in altimetric maps seem to require a priori knowledge of its presence, for instance with the help of previous hydrographic data (Stammer *et al.*, 1991). A study of interactions between a surface turbulence field and a mid-depth eddy has not conclusively provided a criterion for meddy detection at the surface (Quimerc'h & Morvan, 1996). Further investigation is under way in a primitive equation model.

The detectability of deep eddies at the surface, either directly or via their interaction with other flow patterns, thus remains an open subject of great practical interest.

Acknowledgements

Funding for this study was provided by SHOM and DGA under programs FRE 91009401 and PEA 982401. The authors express gratitude to Dr Bach Lien Hua for fruitful discussions. The present results are part of FOV's doctoral dissertation at the Université de Bretagne Occidentale (1999). This work is a contribution to the SEMAPHORE research program.

References

- Barnier, B., Hua, B.L., and Le Provost C., 1991: On the catalytic role of high baroclinic modes in eddy-driven large-scale circulation. *J. Phys. Oceanogr.*, 21, 976-997.
- Bell G.I. and Pratt L.J., 1992: The interaction of an eddy with an unstable jet. *J. Phys. Oceanogr.*, 22, 1229-1244.
- Dritschel, D.G. and Saravanan R., 1994: Three-dimensional quasi-geostrophic contour dynamics, with an application to stratospheric vortex dynamics. *Q. J.R. Meteorol. Soc.*, 120, 1267-1297.
- Flierl G.R., Carton X.J. and Messenger C., 1999: Vortex formation by unstable oceanic jets. Proceedings of the 3rd International Workshop on Vortex Flows, ESAIM, SMAI, 7, 137-150.
- Gould, W.J., 1985: Physical oceanography of the Azores front. *Progress in Oceanography*, 14, 167-190.
- Holland, W.R., 1978: The role of mesoscale eddies in the general circulation of the oceans. Numerical experiments using a wind-driven quasi-geostrophic model. *J. Phys. Oceanogr.*, 8, 363-392.
- Ikeda M. and Lygre K., 1989: Eddy-current interaction using a two-layer quasi-geostrophic model. In "Mesoscale/Synoptic coherent structures in geophysical turbulence". J.C.J. Nihoul and B.M. Jamart eds. Elsevier oceanogr. series, vol.50, 277-291.
- Käse R.H. and Zenk W., 1996: Structure of the Mediterranean water and meddy characteristics in the Northeast Atlantic. In "The Warmwatersphere of the North Atlantic Ocean", ch.12. W. Krauss, Ed. Gebruder Borntraeger, Berlin, 445 pp.
- Kielmann J. and Käse R.H., 1987: Numerical modeling of meander and eddy formation in the Azores current frontal zone. *J. Phys. Oceanogr.*, 17, 529-541.
- LeTraon P.Y., DeMey P., 1994: The eddy field associated with the Azores front east of the Mid-Atlantic ridge as observed by the Geosat altimeter. *J. Geophys. Res.*, 99, 9907-9923.
- Lévy, M., Klein P. and Treguier A.M., 2001: Impacts of sub-mesoscale dynamics on phytoplankton production and subduction. *J. Mar. Res.*, 59, 535-565.
- Morel Y., 1995: Etude des déplacements et de la dynamique des tourbillons géophysiques. Application aux Meddies. Doctorat de l'Université Joseph Fourier, Grenoble I, France, 250 pp.
- Pedlosky J., 1987: *Geophysical Fluid Dynamics*. Springer Verlag. New York.
- Pedlosky J., 1992: Baroclinic instability localized by dissipation. *J. Atmos. Sci.*, 49, 1161-1171.
- Quimerc'h C., Morvan, G., 1996: Interaction d'un tourbillon intrathermocline, de type meddy, avec un champ turbulent de moyenne-échelle". Rapport de fin d'études, ENSIETA, Brest, France, 65 pp.
- Richardson P.L. and Tychensky A., 1998: Meddy trajectories in the Canary Basin measured during the SEMAPHORE experiment, 1993-1995. *J. Geophys. Res.*, 103, C11, 25029-25045.
- Rivière P., 1995: Effets de la friction sur l'instabilité barocline non-linéaire. Thèse, Université de Bretagne Occidentale, Brest, France, 169 pp.
- Stammer D., Hinrichsen H.H. and Käse R.H., 1991: Can meddies be detected by satellite altimetry ? *J. Geophys. Res.*, 96, C4, 7005-7014.

- Stern M.E. and Bidlot J.R., 1994: Lateral entrainment in baroclinic currents, *J. Mar. Res.*, 52, 25-53.
- Stern M.E. and Bidlot J.R., 1995: Lateral entrainment in baroclinic currents, II, *J. Mar. Res.*, 53, 249-267.
- Tychensky A. and Carton X., 1998: Hydrological and dynamical characterization of meddies on the Azores region: a paradigm for baroclinic vortex dynamics. *J. Geophys. Res.*, 103, C11, 25061-25079.
- Tychensky A., Le Traon P.Y., Hernandez F. and D. Jourdan, 1998: Large structures and temporal changes in the Azores front during the Semaphore experiment. *J. Geophys. Res.*, 103, C11, 25009-25027.
- Yano J.I. and Flierl G.R., 1992: Isolated potential vorticity patches in quasi-geostrophic zonal shear flows. *Dyn. Atmos. Oceans*, 16, 439-472.

Figure Captions

Fig. 1:

(a) and (b) Horizontal maps of temperature at 200 m and 1000 m depths and of surface current for the third leg of Semaphore93 experiment. The interaction between the Azores current and the meddy appears at both depths, and a surface cyclone is clearly visible;

(c) Long-term trajectory of meddy after interaction with the Azores Current (Richardson & Tychensky, 1998).

Fig. 2:

Schematic initial conditions of vortex-jet interaction.

Fig. 3:

(a) Potential vorticity maps in both layers at model time $t = 480$ for regime 1 (experiment 1a);

(b) Corresponding scatter-plots $(q, \psi + C_x y)$ for the vortex at model times $t = 60$ (upper plot) and $t = 480$ (lower plot);

(c) Time-series of potential vorticity maps in both layers for regime 2 (experiment 1b); left-hand (right-hand) column is the upper (lower) layer.

Fig. 4:

Linear instability diagrams in the 2-1/2 layer model with $\Delta Q_{J1} = 1, \Delta Q_{J2} = -0.1, \beta = 0$. Solid lines are the growth rates, dashed lines are phase speeds.

(a) the unforced case ($r_1 = r_2 = 0$);

(b) the forced case ($r_1 = r_2 = 0.01$).

Fig. 5:

Time-series of potential vorticity maps in both layers for the interaction of a vortex with a linearly unstable jet in free-decay

(a) f -plane evolution with upper layer (a1) and lower layer (a2), (experiment 2a);

(b) β -plane evolution with upper layer (b1) and lower layer (b2), (experiment 2b).

Fig. 6:

Time-series of potential vorticity maps in both layers for the interaction of a vortex with a linearly unstable jet on the f -plane

(a) unforced simulation with upper layer (a1) and lower layer (a2), (experiment 3a);

(b) forced simulation with upper layer (b1) and lower layer (b2), (experiment 3b).

Fig. 7:

(a) and (b) modal analyses corresponding to experiments 3a and 3b): time evolution of the wave amplitudes in the upper layer, before and after vortex introduction (thick vertical line).

Fig. 8:

As figure 6, with $\beta = 0.029$ (experiments 3c and 3d).

Fig. 9:

(a) and (b) modal analyses corresponding to experiments 3c and 3d.

Fig. 10:

Modal analysis of the upper layer jet for experiment 3e ($\beta = 0.064$).

Fig. 11:

Dominant wavenumbers for the forced experiments with respect to β (a) and to $\gamma_1 R_T$

(b). Blue triangle denotes the stage of jet equilibration; red circle and black square are the first and second largest waves during the jet-vortex interaction.

	ΔQ_{J1} ΔQ_{J2}	ΔQ_{T1} ΔQ_{T2}	$\gamma_1 \ \gamma_2$	y_T	β
<i>experiment 1a</i>	1, 0	0, -0.9	1.3, 3.4	1.9	0
<i>experiment 1b</i>	1, 0	0, -2.01	1.3, 3.4	1.9	0
<i>range of variation</i>	[0, 1] [0, 1]	[-3, 0] [-3, 0]	[1.0, 5.5] [2.4, 3.8]	-	-

Table 1: Values of dimensionless physical parameters for the interaction of a vortex with a stable jet (experiments 1a and 1b); range of variation of physical parameters for the sensitivity study (section 3)

	ΔQ_{J1} ΔQ_{J2}	ΔQ_{T1} ΔQ_{T2}	γ_1, γ_2	y_T	β
<i>experiment 2a</i>	1, -0.1	0, -0.54	1.3, 2.7	2.2	0
<i>experiment 2b</i>	1, -0.1	0, -0.54	1.3, 2.7	2.2	0.029

Table 2: Values of dimensionless physical parameters for the interaction of a vortex with a linearly unstable jet in free-decay (experiments 2a and 2b)

<i>Experiments</i>	r_k	β	n (1)	n (2)
3a	0	0	1, 2 : aperiodic	indeterminate
3b	10^{-3}	0	2 : aperiodic	3
3c	0	0.029	2 : quasi-stationary	2, 4, 3, 1
3d	10^{-3}	0.029	3, 4 : aperiodic	2, 1
3e	10^{-3}	0.064	3, 4 : periodic	2, 3, 1

Table 3: (1) Dominant modes resulting from nonlinear equilibration of unstable jet in isolation; type of dynamical regime obtained; (2) Mode n corresponding to the wavenumbers jet-vortex interaction, $n = (L_x/2\pi)k$.

	ΔQ_{J1} ΔQ_{J2}	ΔQ_{T1} ΔQ_{T2}	γ_1, γ_2	y_T
<i>experiment 3</i>	1, -0.1	0, -0.54	1.3, 2.7	2.2

Table 4: Values of dimensionless physical parameters for the interaction of a vortex with a relaxed, linearly unstable jet (experiments 3a,b,c,d,e)

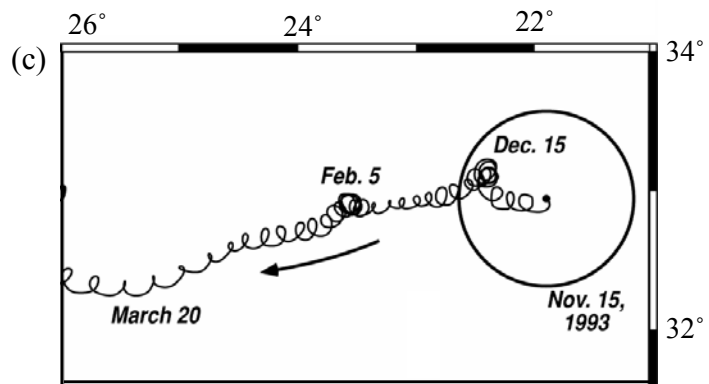
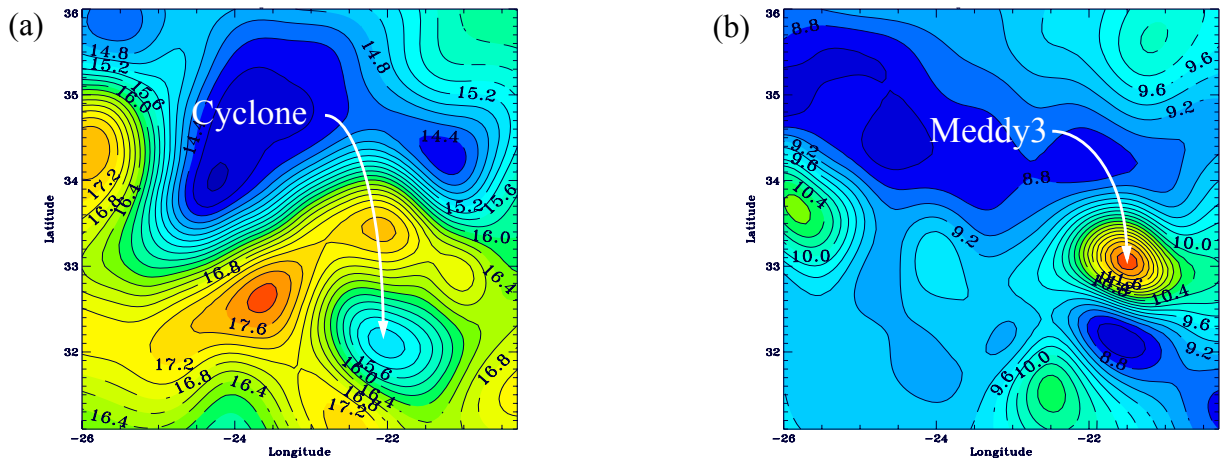


Fig.1

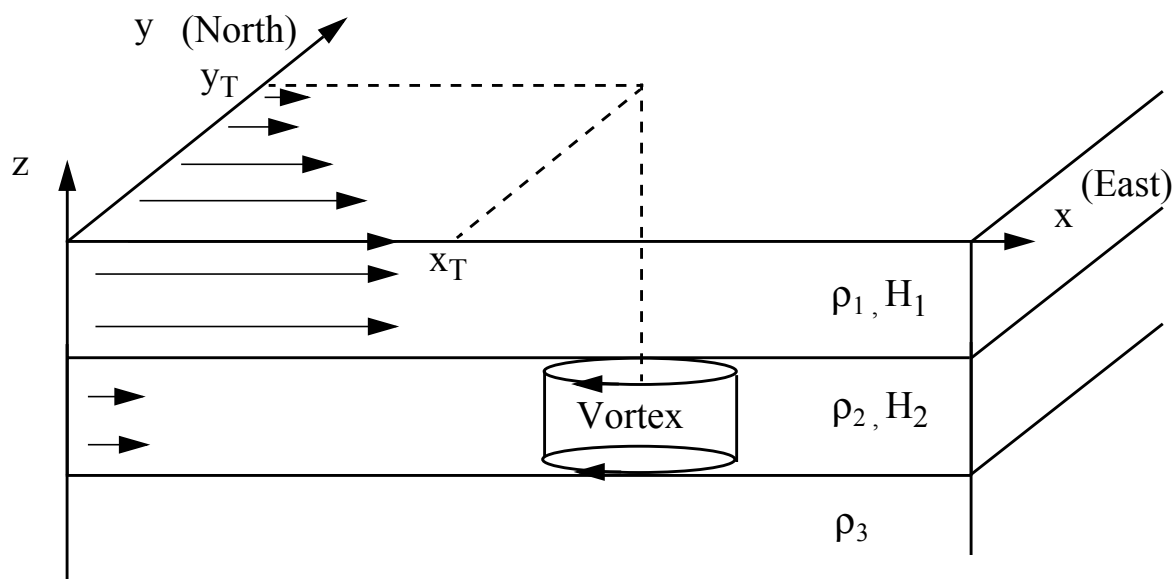


FIG.2

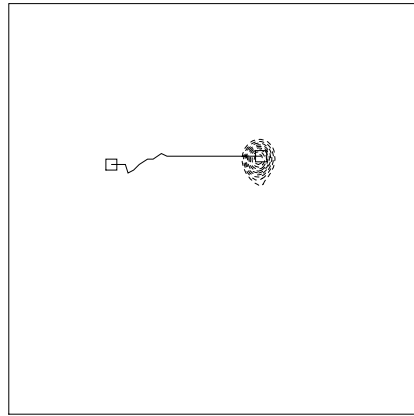
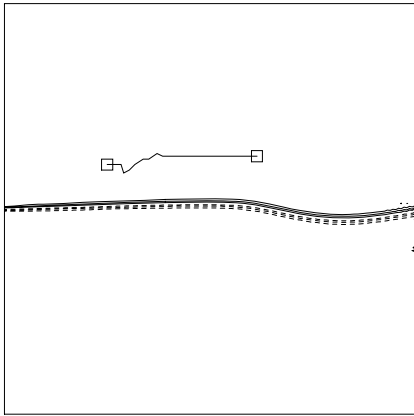


Fig.3a

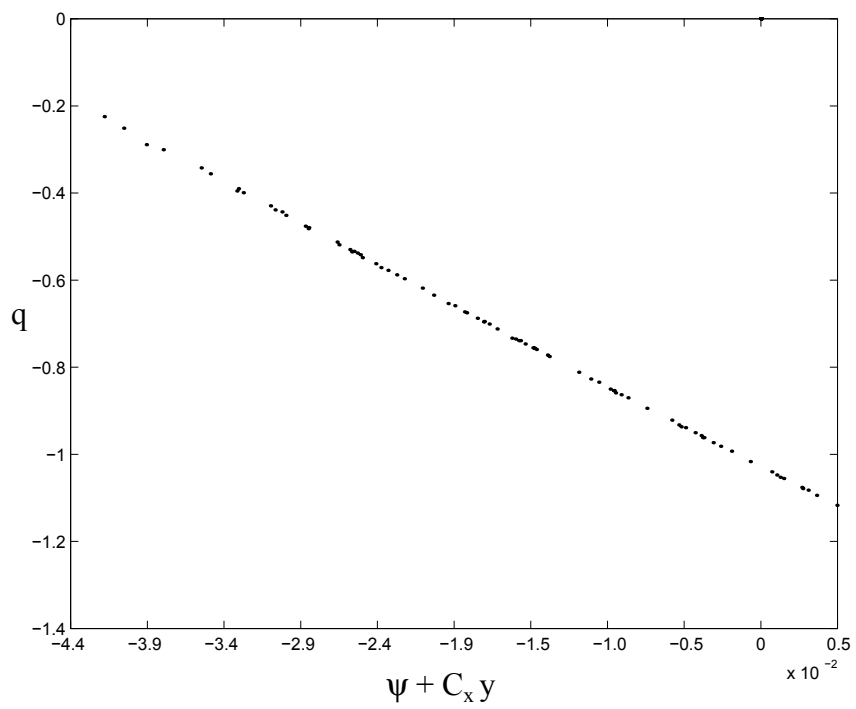
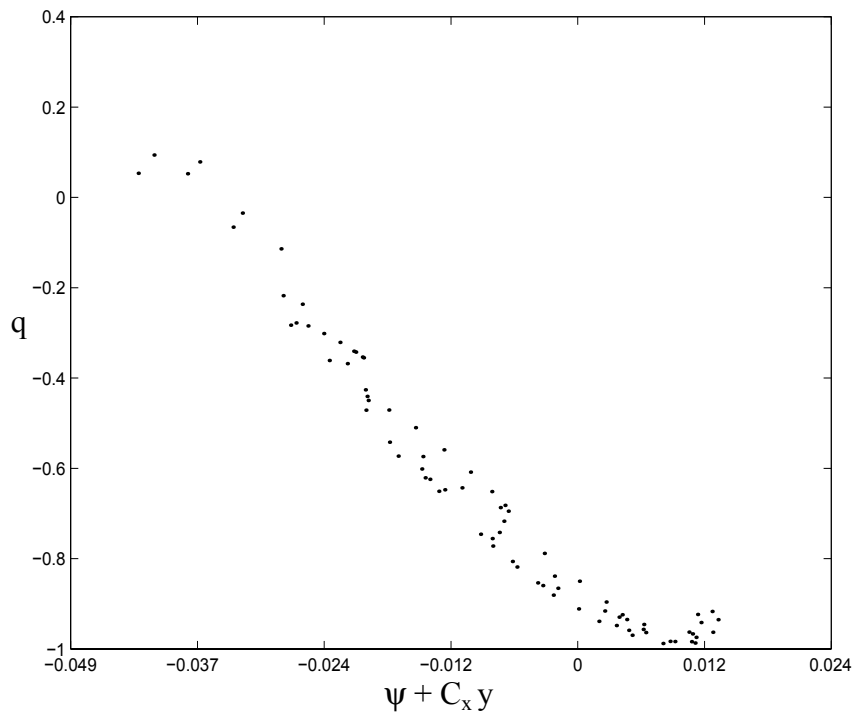


Fig.3b

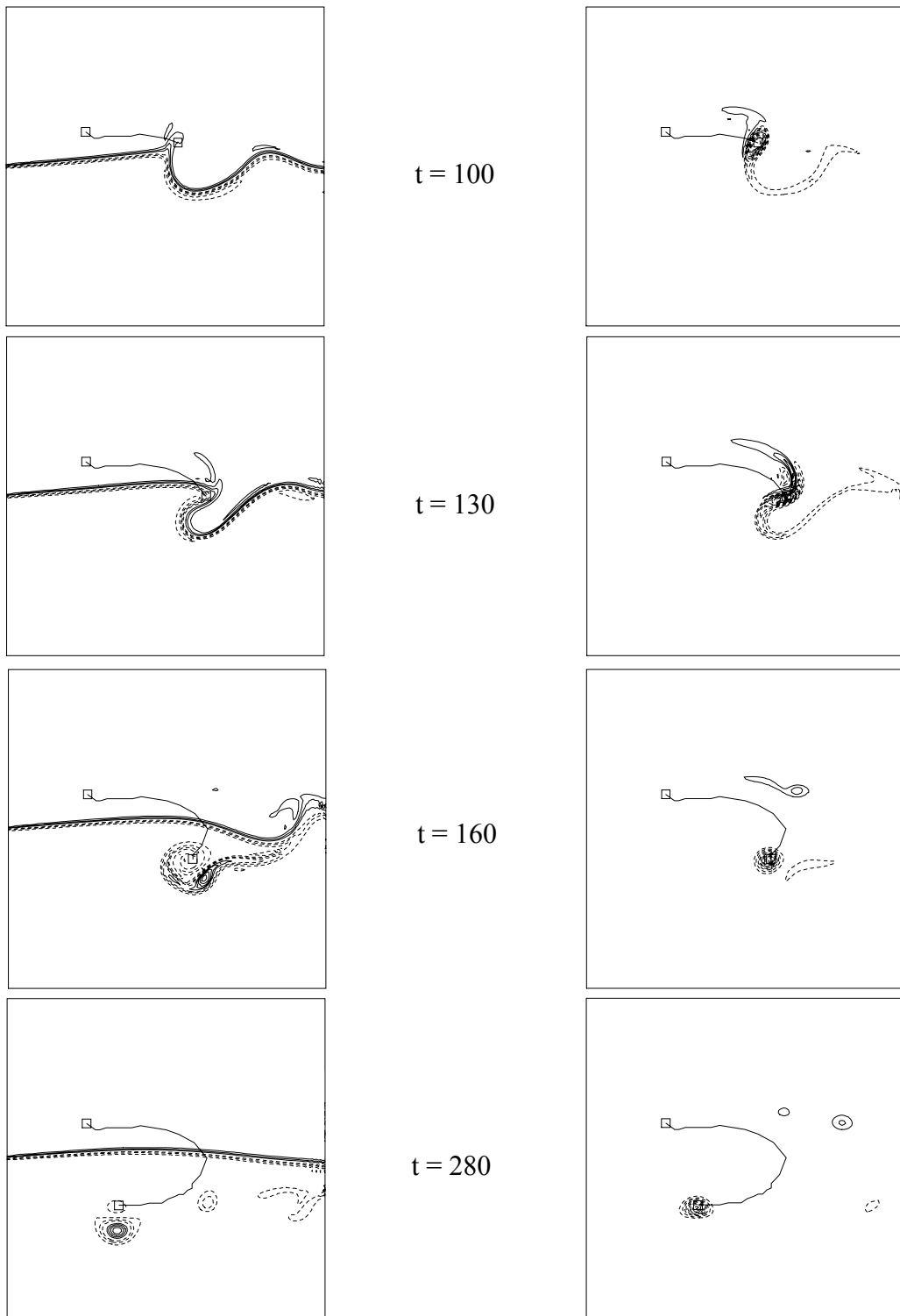


Fig.3c

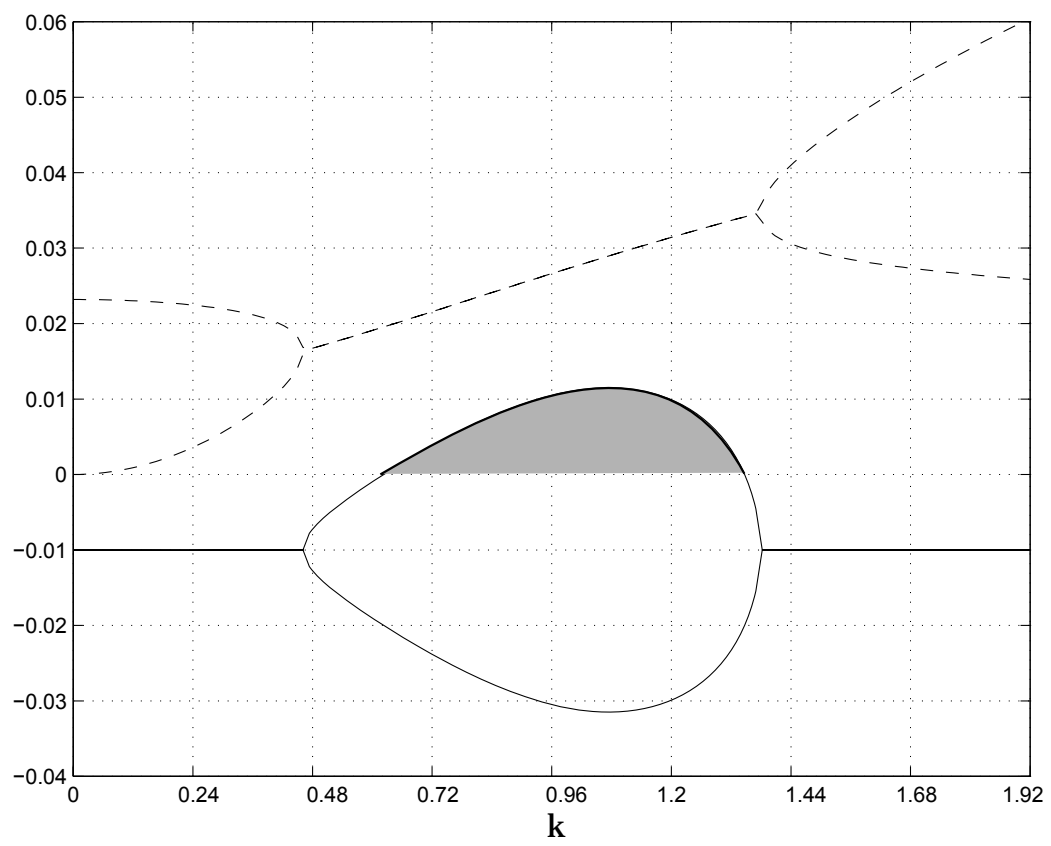
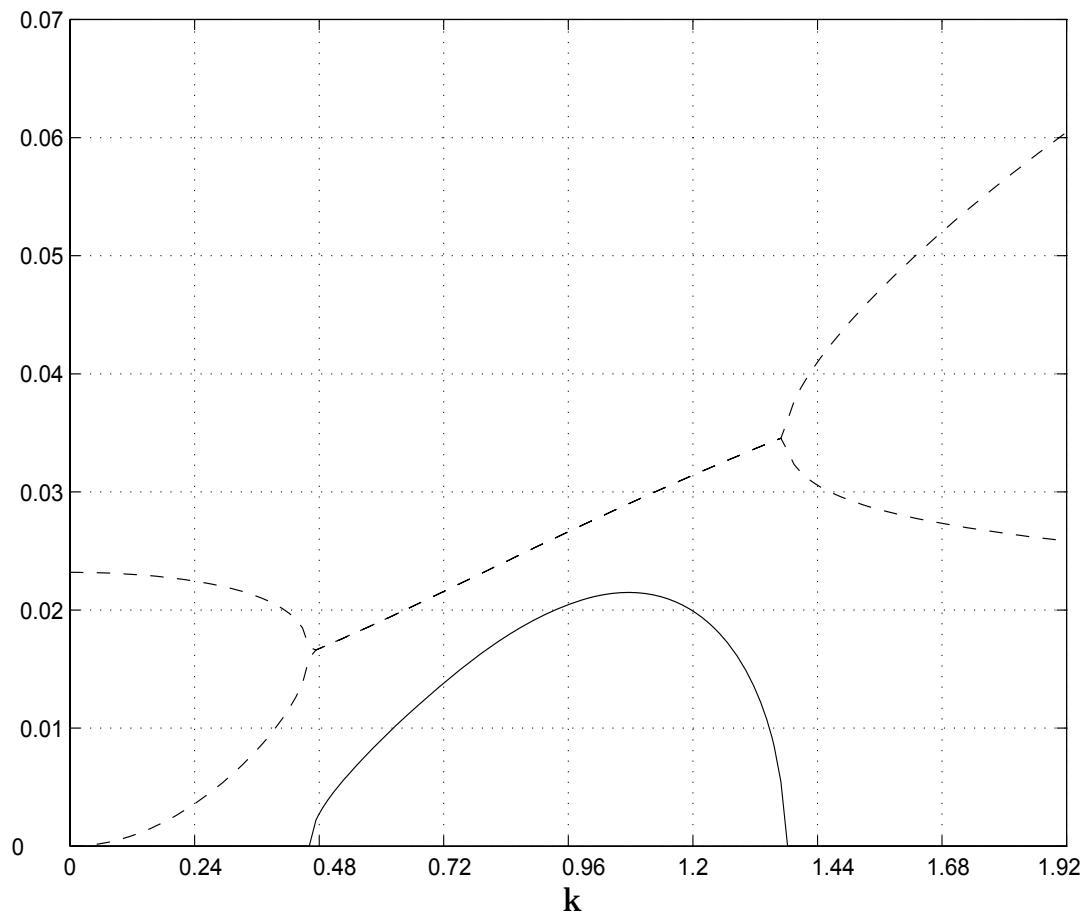


Fig.4

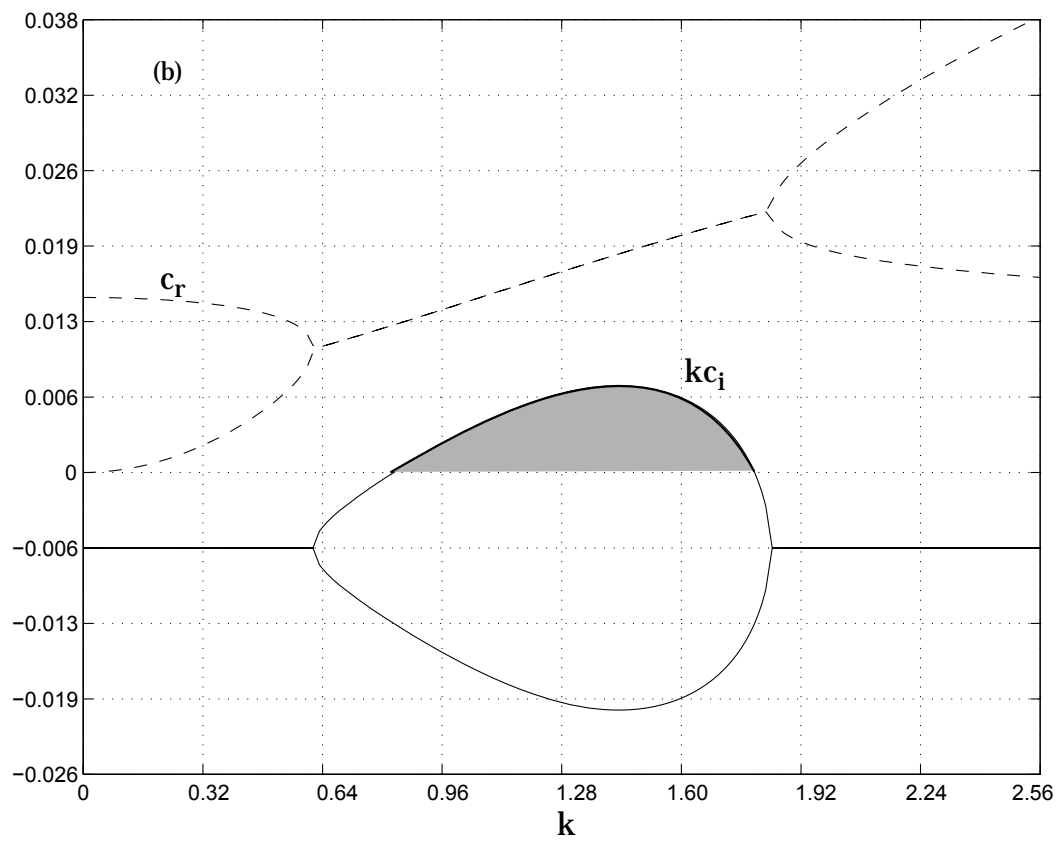
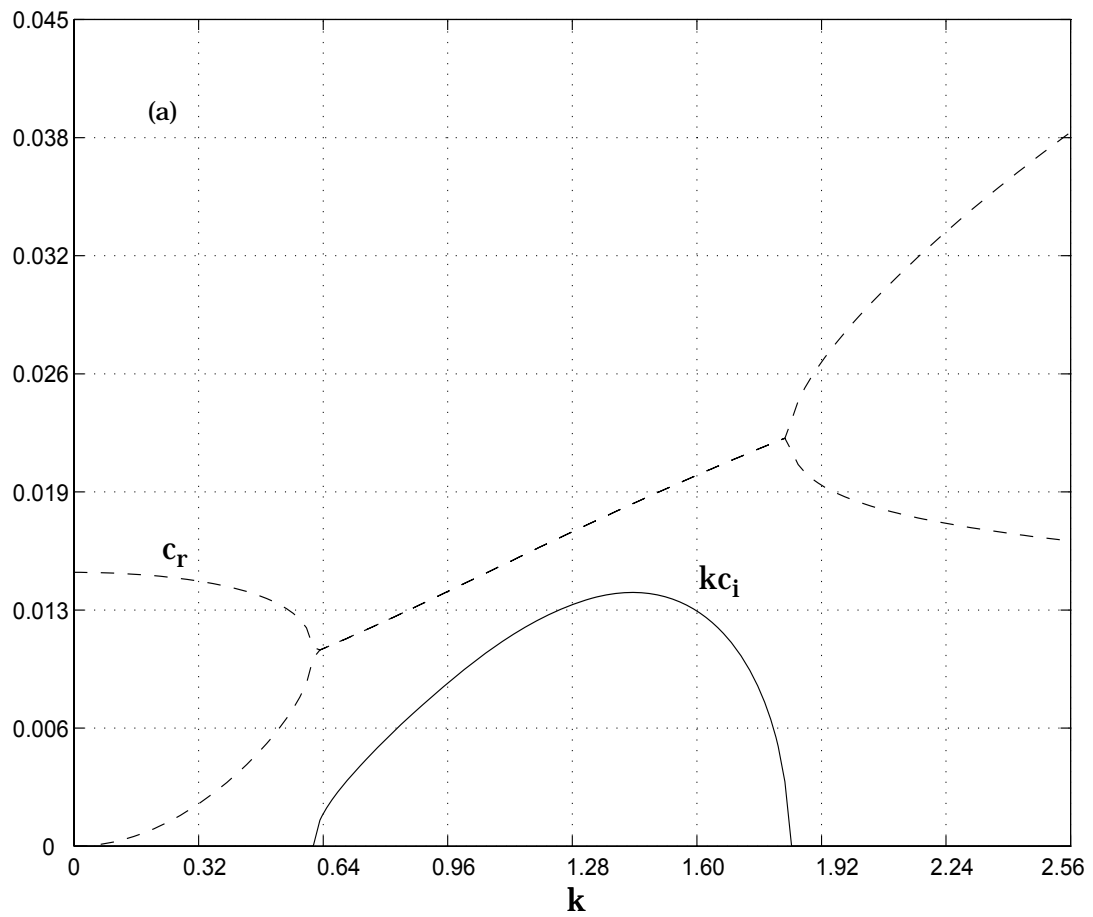
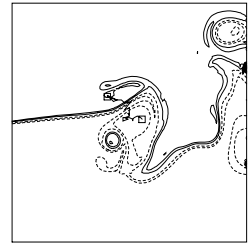
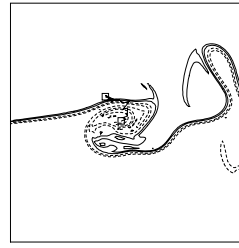
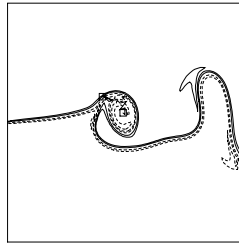
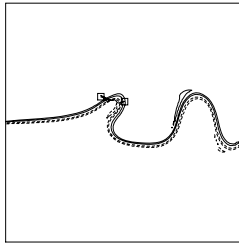
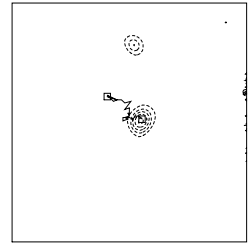
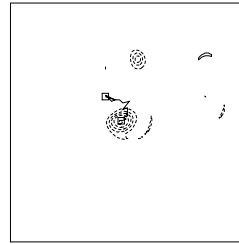
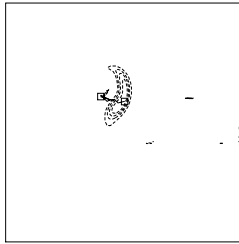


Fig.4a-b

(a1)



(a2)



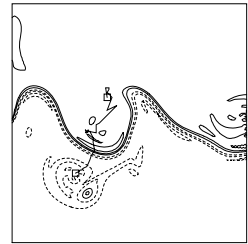
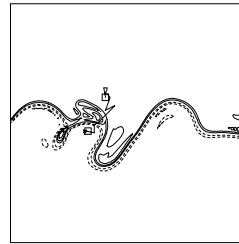
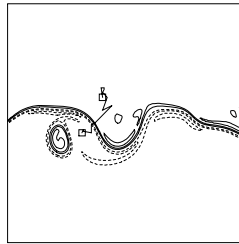
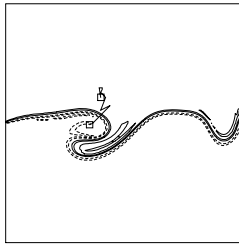
t = 200

t = 280

t = 360

t = 600

(b1)



(b2)

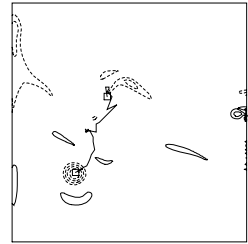
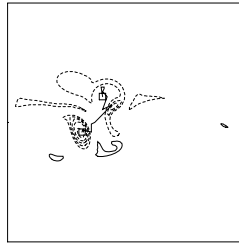
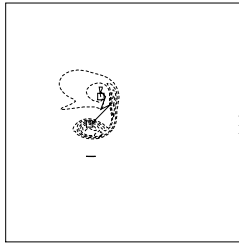


Fig.5a-b

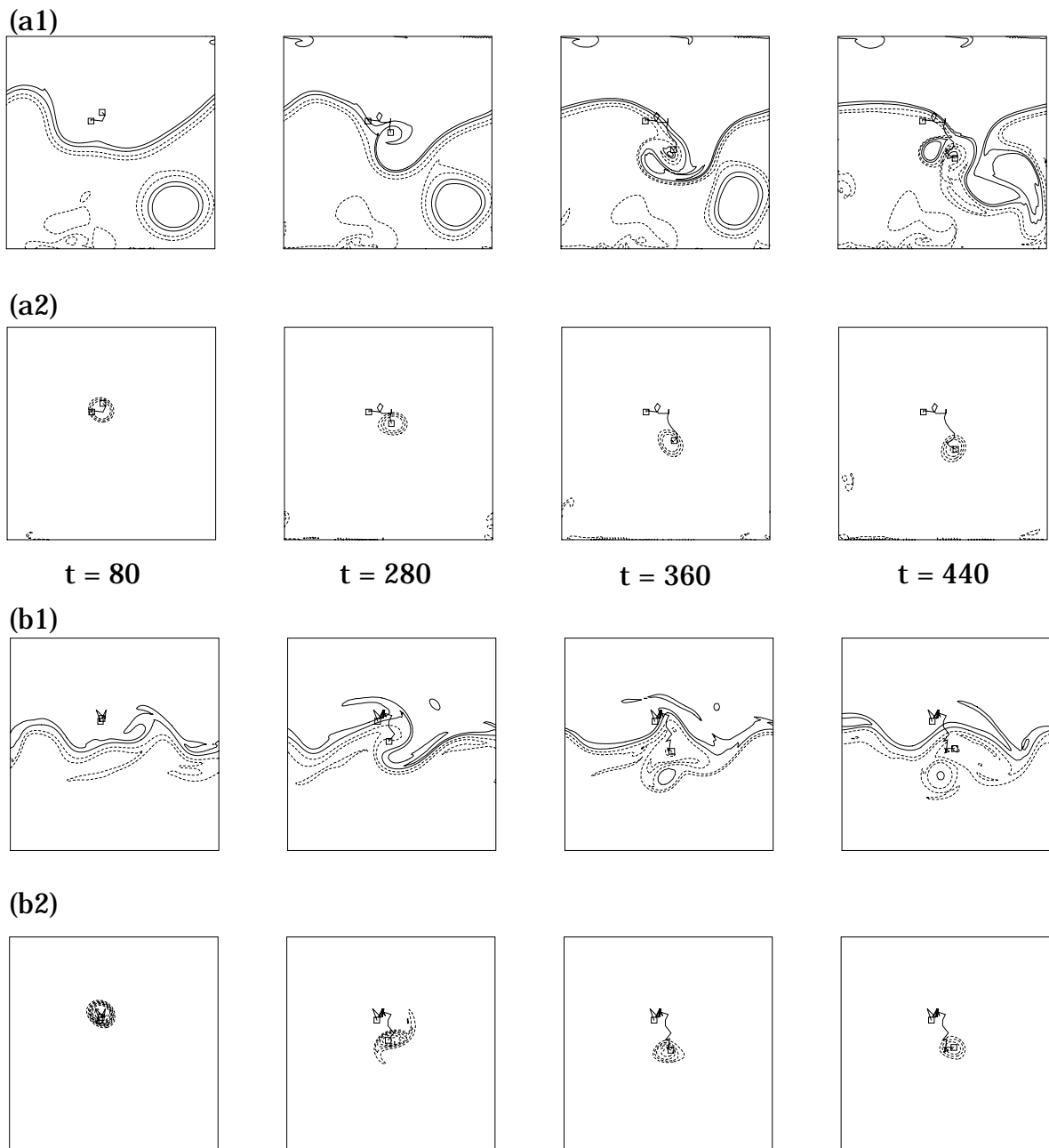
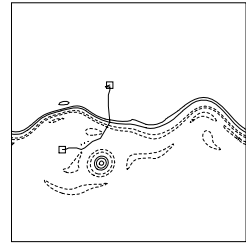
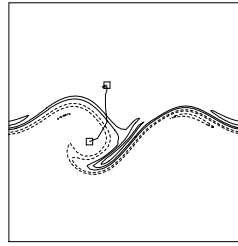
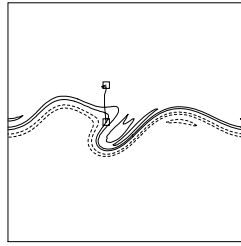
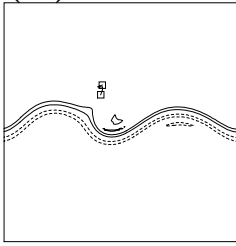


Fig.6a-b

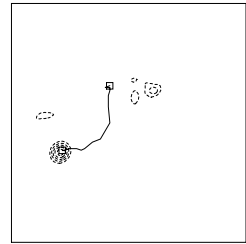
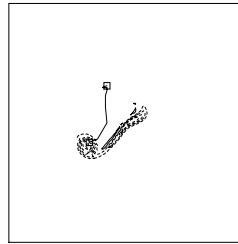
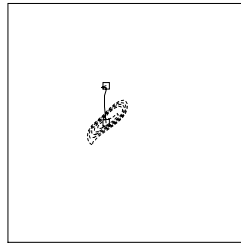
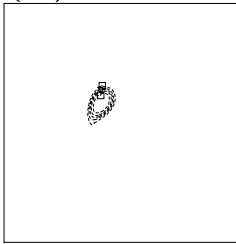


Fig.7a-b

(a1)



(a2)



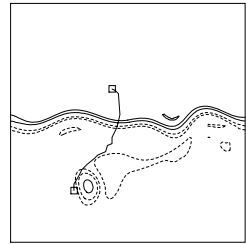
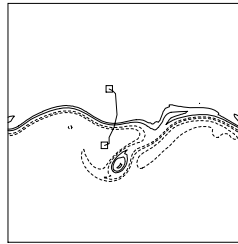
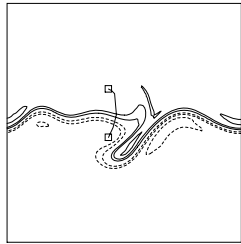
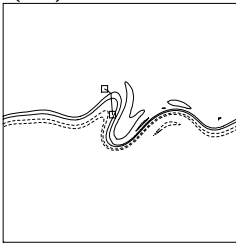
t = 80

t = 120

t = 160

t = 320

(b1)



(b2)

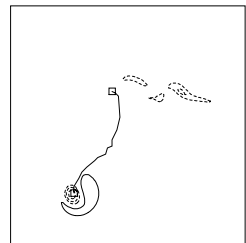
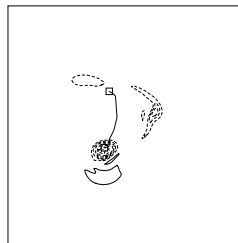
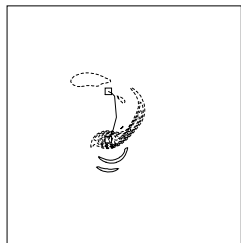
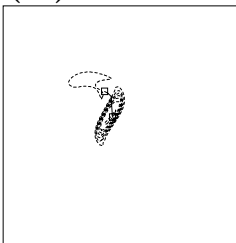


Fig.8a-b

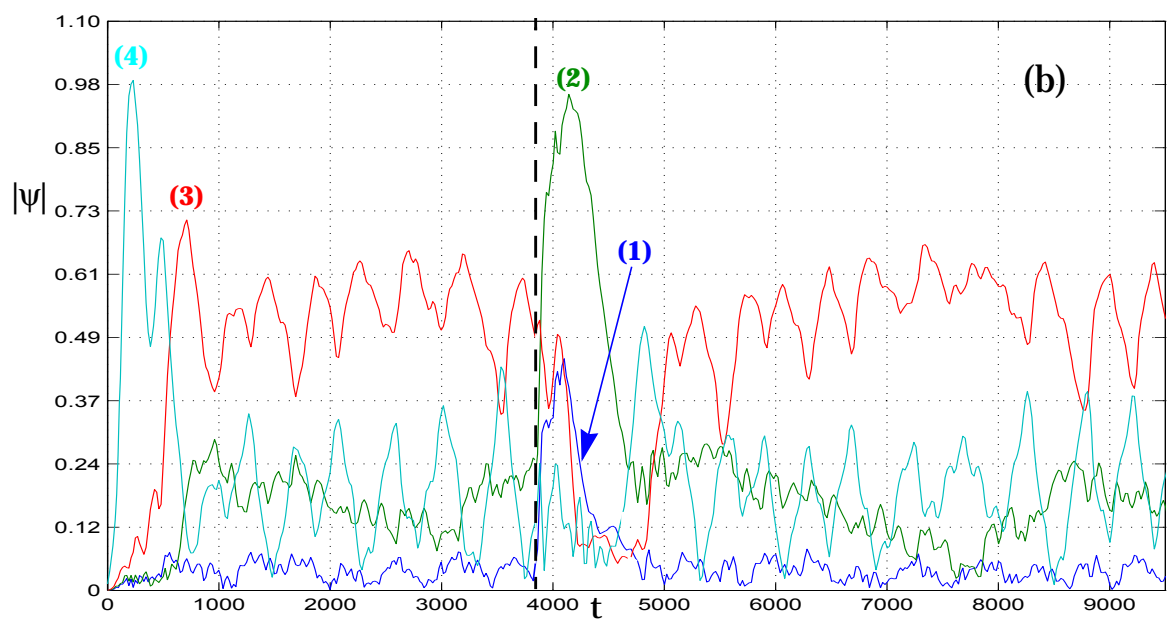
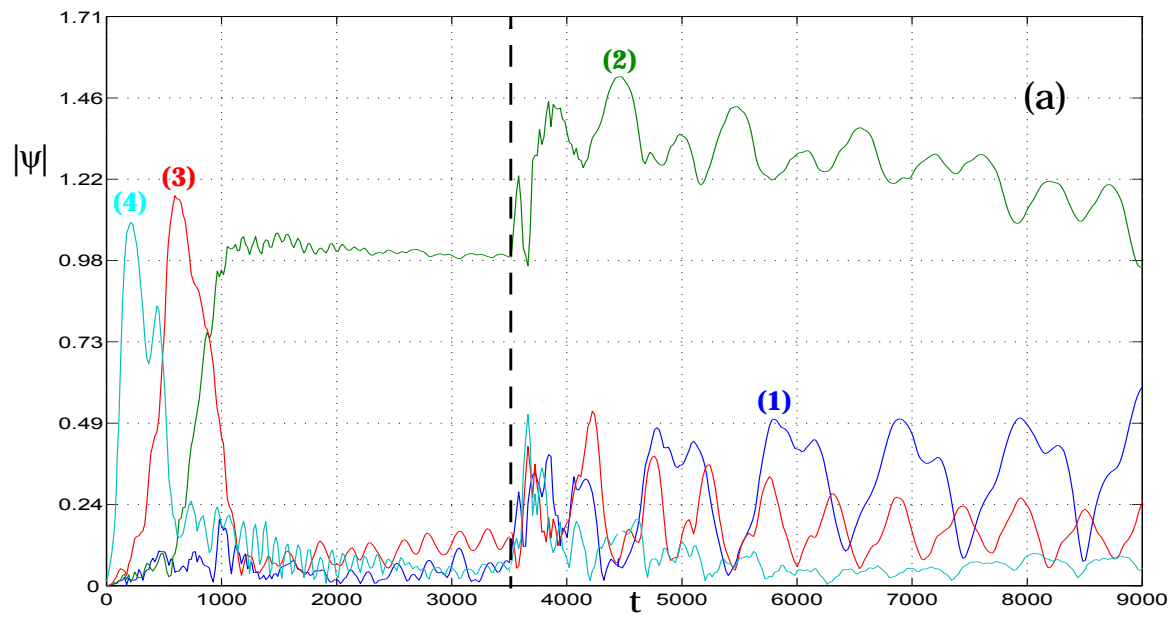


Fig.9a-b

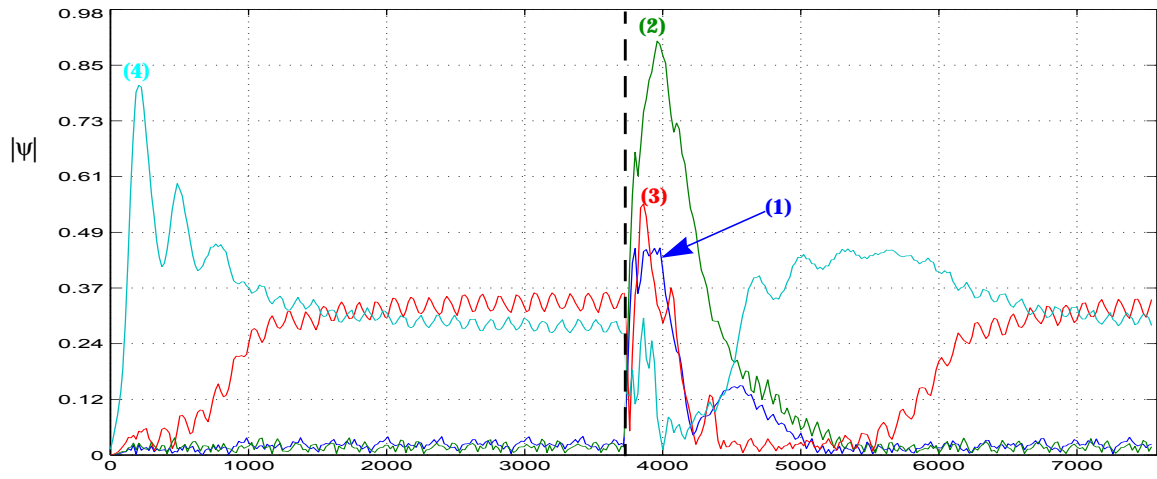


fig 10

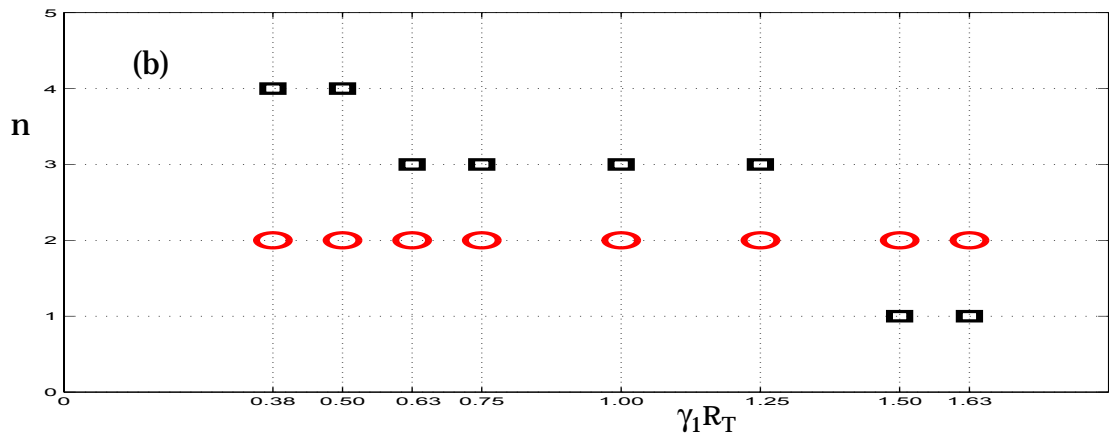
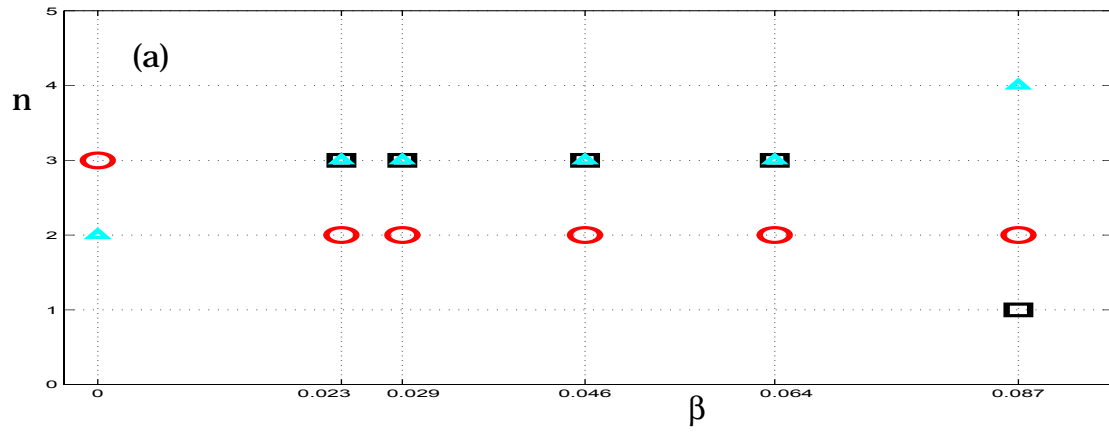


FIG.11a-b